10.1098/rspa.2000.0613

THE ROYAL SOCIETY

Development of a lifting wavelet representation for surface characterization

By X. Q. Jiang, L. Blunt and K. J. Stout

Centre for Precision Technologies, School of Engineering, University of Huddersfield, Huddersfield HD1 3DH, UK

Received 30 March 1999; revised 23 August 1999; accepted 3 November 1999

This paper reviews the existing numerical analysis methods and their problems in surface metrology. Based on the requirements of functional analysis of surfaces, this paper proposes a lifting wavelet representation for extraction of different components of a surface. The theory of the lifting wavelet is introduced and a fast algorithm is developed. Different frequency components of the surface can be separated, extracted and then reconstructed according the intended requirements of functional analysis. The surface textures can be highlighted and multi-scalar topographical features can be identified and clearly recovered. In order to verify the behaviour of the new model, a computer simulation based on sinusoidal and triangular waveforms is used. Case studies are conducted using a series of typical surfaces of engineering and bioengineering, such as planes, cylinders and curves, measured by contact (stylus) and non-contact (phase-shifting interferometry) instruments, to demonstrate the feasibility and applicability of using the lifting wavelet model in the analysis of these surfaces.

Keywords: lifting wavelet; roughness; waviness; form error; multi-scalar topographical features; surface characterization

1. Introduction

It is recognized that surface topography is the one of the most important factors affecting the functional performance of components. The functions that have been identified in various studies include wear, friction, lubrication, corrosion, fatigue, coating, paintability, etc. (Bhushan 1996; Scott 1998; Stout *et al.* 1993; Thomas 1982; Whitehouse 1994). It is also reported that the wear rates of surfaces in operational service is determined by roughness, waviness and the multi-scalar topographic features of a surface, such as random peaks/pits and ridges/valleys. These functional topographical features will impact directly on wear mechanics and physical properties of a whole system, such as a hip joint replacement system in bioengineering (Bachnick *et al.* 1994; Bauer *et al.* 1994; Fisher *et al.* 1994; Hall *et al.* 1996; McGovern *et al.* 1996; Unswoth 1995). For example, during functional operation of interacting surfaces, peaks and ridges will act as sites of high contact stresses and abrasion, and consequently, wear particles and debris will be generated by such surface topographical features, whereas the pits and valleys will affect the lubrication and fluid retention properties. In this situation, a vitally important consideration for functional characterization must be the appropriate separation of the different

components of surfaces, which is not only to extract roughness, waviness and form error, but also should be extended to concern all multi-scalar topographical events over surfaces.

Conventionally, only the extraction of roughness and waviness components of a surface is considered. This is accomplished by using filtering techniques, especially Gaussian filtering (ISO 11562 1994; Stout *et al*. 1993; Whitehouse 1994). These techniques are employed to isolate the roughness frequency band relevant to the surface by the breaking down of a surface signal. These techniques take the waveform created by the surface data as received and decompose it. In fact, Gaussian filtering, used to extract the roughness and waviness components, is based on two presuppositions. One presupposition is that before filtering, the irrelevant form and translation errors have been removed from the measured dataset. The other is that the residual surface, obtained according to the first assumption, can be broken down into a series of harmonic components. If surfaces conform to these assumptions, the roughness and waviness can be well identified and extracted from the original surfaces, though with a modified amplitude resulting from the transmission characteristics of a Gaussian function.

In order to monitor manufacturing processes and identify surface texture, random process techniques have been applied to surface analysis in which the surface topography is assumed as a stationary random system. The spectral and correlation techniques based on the Fourier transform are used to study time-averaging frequency information of surfaces (Nayak 1971). Wallach (1969), Weszka *et al*. (1976), Sato & O-hori (1981) and Sherrington & Smith (1988) applied the areal spectra to diagnoses and analyses of the processes of manufacturing and the machine tool marks of surfaces. Stout *et al*. (1993) demonstrated that the areal spectra provide distinctive spectral patterns to represent the directionality of the surface texture. However, the disadvantage of random analysis is that significant differences involved in a surface, such as large peaks/pits or ridges/valleys, will be smoothed over the space of a signal, without indicating the location of the frequency events.

Identification of topographic features of engineering surfaces has been made by Whitehouse & Zhang (1992; Zhang & Whitehouse 1992). The two possible functions that linked the spatial–spectral domain, the ambiguity function (in radar application) and Wigner distribution (in quantum mechanics) were introduced. Considering that the frequency shift can be preserved in the Wigner distribution and Wigner function has a real-valued capability, whereas the ambiguity function is complex and has a complicated phase property, Whitehouse & Zhang selected the Wigner transform as a tool to investigate the decomposition of the surface signal into a space–frequency plane. The energy distribution in the space–frequency plane, offered by Wigner transform, can be used to identify the variation of a surface topography. The result of this is that the information about the frequencies of a surface signal and their locations has been used to monitor and adjust the manufacturing process. However, it is also well known that although the Wigner transform can offer an analysis of the energy distribution of a signal, it only yields an imperfect descriptor concerning the energy distribution, due to its substantial interference terms. Even now, there does not exist a reasonable algorithm that allows the reconstruction of the atomic decomposition of a signal using the Wigner transform (Meyer 1993).

As previously stated, analysis of multi-scalar properties of a surface topography not only needs to provide both the frequencies of the signal and their location, but is also

expected to accurately recover and perfectly reconstruct these topographic features. Considering the needs of surface assessment, wavelet analysis has been applied to surface characterization (Chen *et al*. 1995; Klimczak & Hanzel-Powierza 1995; Jiang & Li 1994; Jiang *et al*. 1997*a*,*b*, 1998, 1999; Lee *et al*. 1998; Liu *et al*. 1995).

Wavelet analysis employs time–frequency windows and offers the relevant time–frequency analysis, which uses long windows at low frequencies and short windows at high frequencies (shown in figure 2). As a result, 'it can divide functions into different frequency components, and then study each component with a resolution which is matched to its scale' (Daubechies 1992; Chui 1992). This is an alternative to the classical short-time Fourier transform (STFT) or Gabor transform (Gabor 1946; Allen & Rabiner 1977), but there is a basic difference in contrast to STFT, which uses a single analysis window, and offers the same accurate analysis in the whole space–frequency plane. The wavelet transform is related to space–frequency analysis similar to the Wigner–Ville distribution (Wigner 1932). A point to be noted is that wavelet analysis takes the signal decomposition to a space-scalar (time–frequency) plane and separates, then reconstructs these components in the space domain. In contrast, Wigner analysis also decomposes a signal into the space–frequency plane, then studies the energy distribution of these components, but these can not be recovered and reconstructed perfectly. Therefore, taking advantage of the proposed wavelet analysis, the spectral information of the surface topography can be observed on a 'space-scale space', the multi-scalar events over space can be simultaneously tracked and the transient signals along the space can be captured, and later these different components can be perfectly reconstructed.

The wavelet transform has been proved to be a kind of powerful tool for various applications; for example, the wavelet series expansions, developed for pure mathematics and applied mathematics. The multi-scalar feature has been used in capturing, identifying and analysing local non-stationary processes; sub-band coding used in encoding, compressing, reconstructing and modelling signals and images (Daubechies 1988, 1992; Oliensis 1993; Rioul & Vetterli 1991). The wavelet technique includes many different wavelet functions, but each has its own properties and applications. Concerning the need of liner phase (symmetric wavelet) and finite pulse filtering, which are basic properties in surface analysis, only the Haar wavelet and the biorthogonal wavelet have both characteristics. Due to the fact that the Haar wavelet is a binary and discontinuous function (which is not suitable for surface analysis, as indicated by Whitehouse (1994)), only the biorthogonal wavelet looks to have a chance of being a useful tool for surface decomposition. Although the orthogonal wavelet has been used for analysis of a multi-scalar surfaces in engineering by Chen *et al*. (1995), Liu *et al*. (1995) and Jiang & Li (1994), the first two authors neglected the phase distortion, while the latter used an orthogonal wavelet with a high order to improve the phenomenon resulting from phase distortion. This technique led to a large measurement area, a great deal of computation and a huge memory requirement for areal analysis of surfaces.

Biorthogonal wavelet filtering for surface analysis has been proposed by Jiang *et al*. (1997*a*,*b*, 1998, 1999) and has been carried out to directly extract different components from surface topography. The fundamental idea behind the use of this technique is to break down a three-dimensional raw dataset into a rescaled and shifted version of the original waveforms in a 'scalar space', extract the waveforms carrying different information and then reconstruct these components directly. The

main advantage of using a biorthogonal wavelet is that it has a *brick-wall linear phase* (leading to real output without aliasing and phase distortion) and a *traceably located property*, so that the different component surfaces obtained can more naturally record the real surface. However, due to the fact that wavelets $\psi_{j,k}(t)$ (basic functions) are built by dilation and translation of the prototype wavelet $\psi(t)$ which relied on the Fourier transform, and the fact that the wavelet transform needs to be applied along three directions (horizontal, vertical and diagonal) (Mallat 1989; Daubechies 1992), the theory and corresponding algorithm (Mallat 1989; Daubechies 1990, 1992; Chui 1992; Stollntz *et al*. 1996; Strang & Nyguyen 1996) are very complex. Furthermore, there is still the boundary destruction inherent when using the Fourier transform.

For industrial application purposes, the method used for surface functional characterization must have considerable merits. It needs to be simple and natural. In other words, the method of the separation and reconstruction of different components of the surface should have both the 'simplicity' of a Gaussian filter and 'naturalness' of a biorthognal wavelet filter. It is the purpose of this paper to discuss the possibility of using a 'lifting wavelet' representation in an attempt to preserve the above advantages. In this work, the wavelet transform is built using the second generation of biorthogonal wavelet (the so-called lifting wavelet) originally developed at Bell Laboratories in middle of the 1990s (Sweldens 1995, 1996). The wavelet and scalar coefficients are only dependent on the measured raw data of a surface and the filtering and lifting factors calculated by a cubic spline interpolation in an interval (Dyn *et al*. 1987; Flowers 1995; Stoer & Bulirsch 1980). Compared to the former wavelet representation, the new model does not take the Fourier transform as a prerequisite. The wavelet transform only embraces three stages, splitting, prediction and updating. The other advantage derived from the new model is that there is no boundary destruction. Although the implementation of the lifting wavelet is completely different from the former model, it is much easier to understand and perform. In order to account for possible improvements, computer simulation models consisting of some idealized repetitive waveforms will be considered first. A large number of experiments of engineering surfaces (including turning, milling, reaming, grinding, ballising, honing, lapping, polishing, electric discharging, rolling and chemistry processing) and bioengineering surfaces (such as super-lapping, diamond-like coating and UHMWPE) have been carried out. The accuracy of the surfaces of these components covers the levels from the micrometre to nanometre. The specimens include real manufacturing process, running-in and worn surfaces at different stages, as well as standard MICROSURF samples with different machining methods. A group of examples has been selected here to demonstrate the feasibility and applicability of the lifting wavelet for the characterization of surfaces.

2. The biorthogonal wavelet for surface analysis

(*a*) *The first-generation biorthogonal wavelet*

A wavelet is a waveform that has compact support in both the space and frequency domains and whose integral is zero. In wavelet analysis the signal is broken down into rescaled and shifted versions of the original waveform. This then transfers space-based information into scale-based information, which represents the frequency and location properties of the original signal. In one dimension, the wavelets $\psi_{j,k}(t)$ (basis

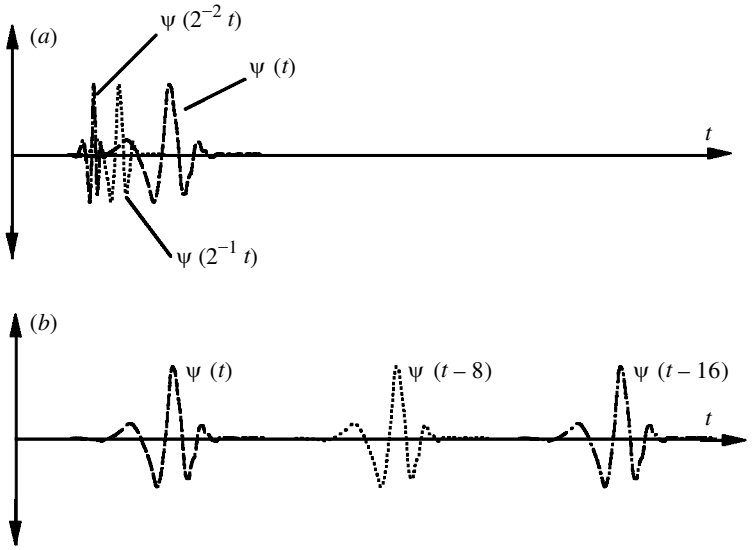

Figure 1. The prototype wavelet and its dilation and translation.
(*a*) The rescaled wavelets $\psi_{j,0}(2^{-j}t)$. (*b*) The shifted wavelets $\psi_{0,k}(t-k)$.

functions) can be obtained by dilation and translation of the prototype wavelet $\psi(t)$. The rescaled wavelets $\psi_{j,0}(t) = \psi(2^{-j}t)$ are dilated by the factor 2^{-j}, as shown in figure 1*a*. j is a scalar parameter that can be used to illustrate wavelets of different widths, or dynamic transmission bandwidths. The shifted wavelets $\psi_{0,k}(t) = \psi(t-k)$ are translated by k (translation parameter), as shown in figure 1*b*. Typical one-dimensional discrete wavelets $\psi_{j,k}(x)$ are dilated j times and shifted k times. The discrete wavelets are expressed by

$$\psi_{j,k}(x) = 2^{-j/2}\psi(2^{-j}x - k). \tag{2.1}$$

Thus a signal is divided into different scales, with the signal data now being represented on a 'space-scalar plane'. Multi-resolution divides the frequencies into octave bands, from ω to 2ω. Frequencies shift upward by an octave when time is rescaled by two. Figure 2 shows how the time–frequency plane is partitioned naturally into rectangles of constant area.

For a discrete signal $y(x) \in L^2(Z)$, its discrete wavelet transform can be expressed by

$$W_{j,k}(y) = \langle y(x), \psi_{j,k}(x)\rangle = 2^{-j/2}\sum_{j,k} y(x)\psi(2^{-j}x - k). \tag{2.2}$$

It was shown by Daubechies (1992) and Chui (1992) that the discrete wavelet transform is reversible. So the signal $y(x)$ can be recovered with the following equation

$$y(x) = \langle y(x), \psi_{j,k}(x)\rangle \Psi_{j,k}(x), \tag{2.3}$$

where $\Psi_{j,k} = (F^*F)^{-1}\psi_{j,k}$. The main approach to the wavelets uses a two-channel filter bank, and the dilation equations of the basis wavelets and corresponding scaling functions develop low-pass H_0 and high-pass H_1 filter coefficients. However, due to

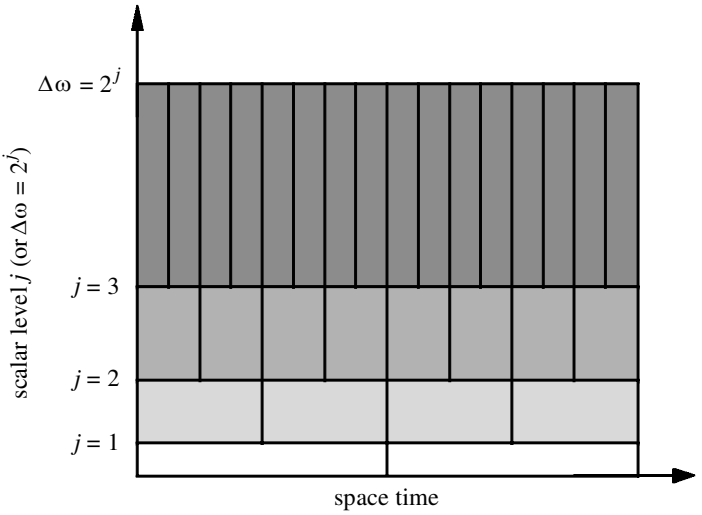

Figure 2. A space-scalar (time–frequency) plane.

the fact that the frequency responses of the two-channel filters, so-called analysing filters, are not ideal brick-wall filters, normally there are overlaps that would lead to aliasing, amplitude modification and phase distortion. In order to overcome these defects, other two-channel filters, G_0 and G_1 (so-called synthesis filters), have been specially designed to compensate for the errors of the analysing filters H_0 and H_1. When the frequency responses of the synthesis filters $G_0(z)$, $G_1(z)$ are the inverses of the analysis filters $H_0(z)$, $H_1(z)$ and they satisfy (Strang & Nguyen 1996)

$$\left.\begin{aligned} G_0(z)H_0(z) + G_1(z)H_1(z) &= 2z^{-l}, \\ G_0(z)H_0(-z) + G_1(z)H_1(-z) &= 0, \end{aligned}\right\} \tag{2.4}$$

the errors in this analysis bank are cancelled. Here, l is time delay, the distortion term must be z^{-l} and the aliasing term must be zero. This means that the two-channel filter banks should be biorthogonal. In the biorthogonal case, the impulse responses $h_0(k)$, $h_1(k)$ of analysis filters would not be double-shift orthogonal to themselves, but they would be double-shift biorthogonal to $g_0(k)$, $g_1(k)$ of the synthesis filters.

According to wavelet theory (Chui 1992; Daubechies 1992), the dilation equations of the analysis wavelet equation $\tilde{\psi}(x)$ and synthesis wavelet function $\psi(x)$ can be performed in the light of the impulse responses of the analysis and synthesis high-pass filters, respectively,

$$\left.\begin{aligned} \tilde{\psi}(x) &= \sum_0^N 2h_1(l)\tilde{\varphi}(2x-l), \\ \psi(x) &= \sum_0^{\tilde{N}} 2g_1(k)\varphi(2x-k). \end{aligned}\right\} \tag{2.5}$$

The scale equation can be given by

$$\left.\begin{aligned}\tilde{\varphi}(x) &= \sum_{0}^{\tilde{N}} 2h_0(l)\tilde{\varphi}(2x-l),\\ \varphi(x) &= \sum_{0}^{N} 2g_0(k)\varphi(2x-k).\end{aligned}\right\} \tag{2.6}$$

The $\tilde{\varphi}(x)$, $\tilde{\psi}(x)$, $\varphi(x)$ and $\psi(x)$ are constructed as a biorthogonal wavelet pair; their limit functions would inherit biorthogonality. A complete study of the first-generation wavelet for surface characterization was carried out by Jiang *et al.* (1999).

(*b*) *The second-generation biorthogonal wavelet*

Due to the significant merits of the biorthogonal wavelet, which allows the construction of symmetric wavelets and thus a linear phase filter, its second-generation algorithm has been developed at Bell laboratories (Sweldens 1995, 1996). The second generation uses the lifting scheme (Sweldens 1994) to replace the Fourier transform as its construction tool and gives up the dilation and translation, but it still preserves all properties of the first-generation algorithm. In this implementation, the analysis high-pass filter H_1 and synthesis low-pass filter G_0 of the initial finite biorthogonal wavelet filter set $\{H_0, H_1, G_0, G_1\}$ within the first generation are transferred to H_1', G_0', which can be found by the lifting scheme as

$$\left.\begin{aligned}H_1'(z) &= H_1(z) + G_1(z)S(z^2),\\ G_0'(z) &= G_0(z) - H_0(z)S(z^{-2}),\end{aligned}\right\} \tag{2.7}$$

where $S(z)$ is a Laurent polynomial. Substituting this new set into (2.4), the perfect reconstructed condition for the second-generation biorthogonal wavelet is

$$\begin{aligned}&G_0'(z)H_0(z) + G_1(z)H_1'(z)\\ &\quad= G_0(z)H_0(z) - H_0^2(z)S(z^{-2}) + G_1(z)H_1(z) + G_1^2(z)S(z^2)\\ &\quad= G_0(z)H_0(z) + G_1(z)H_1(z) + G_1^2(z)S(z^2) - H_0^2(z)S(z^{-2})\\ &\quad= 2z^{-l}\end{aligned} \tag{2.8}$$

and

$$\begin{aligned}&G_0'(z)H_0(-z) + G_1(z)H_1'(-z)\\ &\quad= G_0(z)H_0(-z) - H_0(z)H_0(-z)S(z^{-2}) + G_1(z)H_1(-z) + G_1(z)G_1(-z)S(z^2)\\ &\quad= G_0(z)H_0(-z) + G_1(z)H_1(-z) + G_1(z)G_1(-z)S(z^2) - H_0(z)H_0(-z)S(z^{-2})\\ &\quad= 0.\end{aligned} \tag{2.9}$$

In order to perfectly reconstruct, the frequency responses of the analysis and synthesis filters of the second algorithm should be also satisfied,

$$\left.\begin{aligned}G_1^2(z)S(z^2) - H_0^2(z)S(z^{-2}) &= 0,\\ G_1(z)G_1(-z)S(z^2) - H_0(z)H_0(-z)S(z^{-2}) &= 0,\end{aligned}\right\} \tag{2.10}$$

except for (2.4). In this case, $S(z^2) = S(z^{-2})$. After lifting has been performed, the new biorthogonal wavelet pair can be found by

$$\left.\begin{aligned} \tilde{\psi}'(x) &= \tilde{\psi}(x) - \sum_{0}^{\tilde{N}} s(l)\tilde{\varphi}(x-l), \\ \psi'(x) &= 2\sum_{0}^{\tilde{N}} g_1(k)\varphi'(2x-k) \end{aligned}\right\} \tag{2.11}$$

and

$$\left.\begin{aligned} \tilde{\varphi}(x) &= 2\sum_{0}^{\tilde{N}} h_0(l)\tilde{\varphi}(2x-l), \\ \varphi'(x) &= 2\sum_{0}^{N} g_0(k)\varphi'(2x-k) + \sum_{0}^{\tilde{N}} s(k)\psi'(x-k), \end{aligned}\right\} \tag{2.12}$$

where the coefficients $s(\cdot)$ are from the Laurent polynomial $S(z)$. The power behind the lifting scheme is that $s(\cdot)$ can be used to fully control all wavelets and synthesis scaling functions.

A simple example is that the linear subdivision ($N = \tilde{N} = 2$) can be obtained by lifting from the Lazy wavelet, which only subsamples the original signal $A_0(x, y)$, in even $A_{0,2k}$ and odd $A_{0,2k+1}$ samples. The Lazy wavelet is the simplest biorthogonal wavelet with $N = \tilde{N} = 0$. If a linear subdivision occurs $N = 2$ after lifting the coefficients $s(l) = (\frac{1}{2}, \frac{1}{2})$, the wavelet coefficient $d_{1,k}$ encodes the difference between the exact sample $A_{0,2k+1}$ and its linear prediction of two even neighbours $A_{0,2k}$, $A_{0,2k+2}$. It can be written as

$$d_{j,k} := A_{j-1,2k+1} - \tfrac{1}{2}(A_{j-1,2k} + A_{j-1,2k+1}). \tag{2.13}$$

Employing the dual lifting scheme, $\tilde{N} = 2$, that is, the coefficient $s'(k) = (\frac{1}{4}, \frac{1}{4})$, the scalar coefficients $a_{1,k}$ of $A_{0,2k}$ would be updated by wavelet coefficients $d_{1,k}$ and $d_{1,k+1}$. This can be expressed as

$$a_{j,k} = A_{j-1,2k} + \tfrac{1}{4}(d_{j,k} + d_{j,k+1}). \tag{2.14}$$

3. The lifting wavelet algorithm

The significant point for the second algorithm is that the wavelet transform is no longer the dilation and translation of a fixed function. The wavelet can be built by the selection of an appropriate Laurent algorithm $S(z)$. Considering the requirements of surface analysis (an excellent refinement accuracy, a perfect reconstruction, a minimum sampling condition (measured area) and a minimum computation), the cubic spline interpolation has been selected to build a new wavelet model.

In the light of the lifting wavelet representation, the sequence for surface analysis is to initially decompose an original surface signal $z(x, y)$ to a sequence of subsets, without an assessment of the frequency content of the original signal. It transfers space-based information into scale-based information, which provides not only frequency events of $z(x, y)$, but also records their location properties completely in the

scalar domain. Next, the different frequency components involved in $z(x, y)$ can be interrogated via a flexible transmission bank according to the intended functional inferences which need to be drawn from it. Finally, the required surfaces can be reconstructed in the spatial domain.

(*a*) *The wavelet transform*

In this wavelet model, a surface topographical signal $z(x, y)$ is assumed to be $A_j(x, y) = z(x, y)$, $j \in Z$; the wavelet transform firstly divides the signal into 'even' and 'odd' subsets, $A_{j,2k}$ and $A_{j,2k+1}$, in which each sequence contains half as many samples as $z(x, y)$, and the operator can be assumed by

$$\left.\begin{aligned} a_{j+1,k} &:= A_{j,2k}, \\ d_{j+1,k} &:= A_{j,2k+1}. \end{aligned}\right\} \tag{3.1}$$

There are no restrictions on the relative size of each part. $a_{j+1,k}$ is a sequence of scalar coefficients and $d_{j+1,k}$ is a sequence of wavelet coefficients. Considering the presupposition of the decomposition is to separate the frequency components of $z(x, y)$ at the scale $2^{-(j+1)}$, both scalar and wavelet coefficients are expected to represent high- and low-frequency information at the scale $2^{-(j+1)}$ of $z(x, y)$, respectively. To fulfil this objective, the scalar and wavelet coefficient sequences $a_{j+1,k}$, $d_{j+1,k}$ are defined by

$$\left.\begin{aligned} d_{j+1,k} &= A_{j,2k+1} - \rho(A_{j,2k}), \\ a_{j+1,k} &= A_{j,2k} + \mu(d_{j+1,k}). \end{aligned}\right\} \tag{3.2}$$

Here, $\rho(A_{j,2k})$ is a weighting prediction of a wavelet coefficient point given by

$$\rho(A_{j,2k}) = \sum_{i=1}^{N} f_i(A_{j,2k}). \tag{3.3}$$

The value of $\rho(A_{j,2k})$ is based on the 'even set' of $z(x, y)$, where N denotes how many data points will attend the weighting prediction. The f_n are a set of filtering factors (weighting function) of one wavelet coefficient point, and can be found by employing a *Neville's polynomial interpolation* with a degree $(N - 1)$ with the following recursion (Dyn *et al.* 1987; Flowers 1995; Stoer & Bulirsch 1980):

$$f_i = f_{1,2,\ldots,N}(x) = \frac{(x - x_1) f_{2,\ldots,N}(x) - (x - x_N) f_{1,2,\ldots,N-1}(x)}{x_N - x_1}. \tag{3.4}$$

The initial coefficients $f_1, f_2, \ldots, f_N$ are a set of Bezier coefficients of a spline interpolation with degree $(N - 1)$. For example, if a prediction of wavelet coefficients is simply a linear subdivision $N = 2$, the weighting prediction can be calculated by using two neighbours; one neighbouring point, $A_{j,2k}$, $A_{j,2k+2}$, on each side (see figure 3*a*). The result is $f_1 = f_2 = \frac{1}{2}$ and

$$d_{j+1,k} = A_{j,2k+1} - \tfrac{1}{2}(A_{j,2k} + A_{j,2k+2}).$$

It is easy to see that the result is equal to (2.13). Considering raw signal data derived from an arbitrarily curved surface in a given space interval, the implementation of a lifting wavelet is to employ a cubic spline interpolation to create a weighting function.

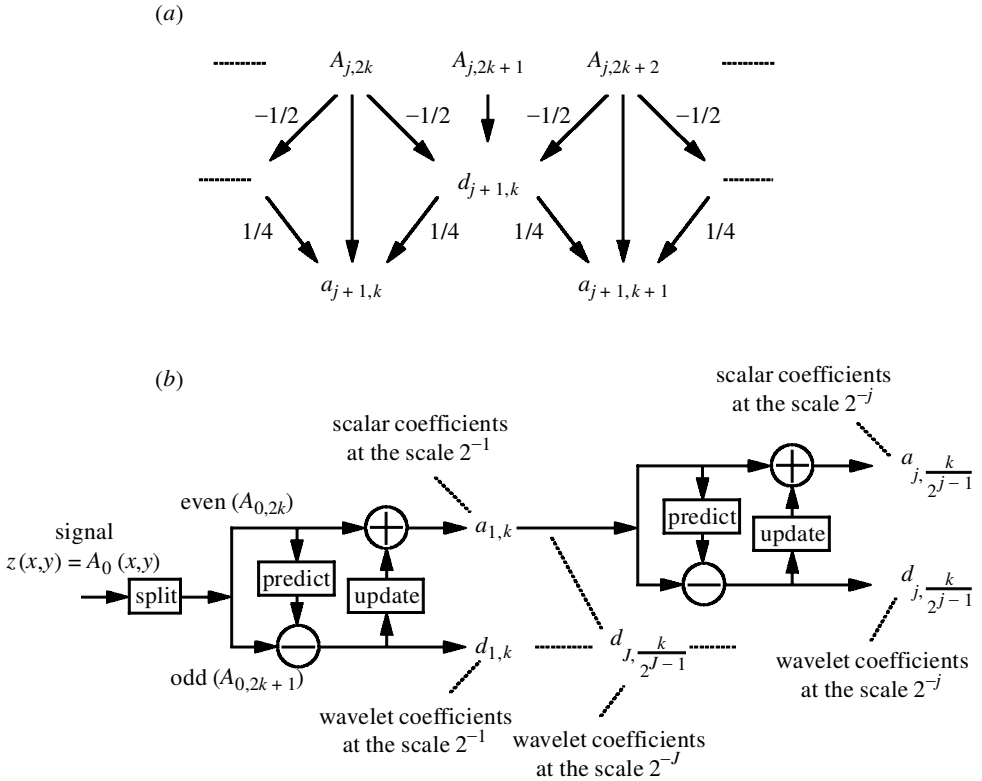

Figure 3. The basic principle of the lifting wavelet. (*a*) The lifting scheme: splitting, prediction and updating. (*b*) The decomposition of $z(x, y)$.

In this case, four neighbouring values will attend a weighting prediction. The only difference between this case and the linear case is that here two neighbouring points on either side are adjusted instead of one. Three cases should be taken into account:

(1) two neighbouring points on either side of an interval;

(2) one sample point on the left and three on the right at the left boundary of an interval; and

(3) vice versa at the right boundary.

These cases are considered in order to guarantee boundary 'naturalness' without including any artefacts (all filtering factors are indicated in table 1). The result of this is that running-in and running-out lengths of normal filtering techniques are not needed. When the prediction value $\rho(A_{j,2k})$ is subtracted from the 'odd set' $A_{j,2k+1}$ of $z(x, y)$, the $d_{j+1,k}$ become a real wavelet coefficient series, and they represent the high-frequency component at scale $2^{-(j+1)}$ of $z(x, y)$.

The $\mu(d_{j+1,k})$ is a weighting update given by

$$\mu(d_{j+1,k}) = \sum_{i=1}^{\tilde{N}} l_i(d_{j+1,k}). \tag{3.5}$$

Table 1. *Filtering factors obtained by Neville's spline interpolating*

cubic spline interpolation		filtering factors					
neighbour number on the left	neighbour number on the right	$k-5$	$k-3$	$k-1$	$k+1$	$k+3$	$k+5$
1	3	—	—	0.3125	0.9375	−0.3125	0.0625
2	2	—	−0.0625	0.5625	0.5625	−0.0625	—
3	1	0.0625	−0.3125	0.9375	0.3125	—	—

It is based on the real wavelet coefficients, where $\tilde{N}$ indicates how many wavelet coefficient points will attend the weighting update. The l_i are referred to as lifting factors. The lifting factors can be calculated from the following algorithm. Firstly, an initial moment matrix for all coefficients at the first level is defined. The matrix aims to preserve the value of the integral of a lifting wavelet along the real line as zero (see Sweldens 1995; Strang & Nyguyen 1996). The moment matrix is only relative to the sampling matrix size of $z(x, y)$ and wavelet coefficient points attending a weighting update,

$$M[p,q] = \begin{bmatrix} m_{1,1} & \cdots & m_{1,\tilde{N}} \\ \vdots & m_{p,q} & \vdots \\ m_{s,1} & \cdots & m_{s,\tilde{N}} \end{bmatrix} = \begin{bmatrix} 1 & 1^2 & \cdots & 1^{\tilde{N}} \\ 2 & 2^2 & & 2^{\tilde{N}} \\ \vdots & & \ddots & \vdots \\ s & s^2 & \cdots & s^{\tilde{N}} \end{bmatrix}, \quad 1 \leqslant p \leqslant s, \quad 1 \leqslant q \leqslant \tilde{N}, \tag{3.6}$$

where s is a sampling number in the processing direction, x or y of $z(x, y)$. Updating the moment matrix requires an indication of how many filtering factors of corresponding wavelet coefficients will be contributed to by this update. When neighbouring point numbers on each side are same, the moments can be expressed by

$$m_{2p,q} = m_{2p,q} + \sum_{t,i} f_i^* m_{t,q}, \tag{3.7}$$

where

$$t = \underbrace{2p-(N-1),\ 2p-(N-1)-2,\ \ldots,\ 2p+(N-1)}_{N}, \quad i = 1, 2, \ldots, N.$$

Therefore, lifting factors are solved using the following linear system:

$$\begin{bmatrix} m_{2p-\tilde{N}+2,1} & \cdots & m_{2p+\tilde{N},1} \\ \vdots & \vdots & \vdots \\ \vdots & m_{2p,q} & \vdots \\ m_{2p-\tilde{N}+2,\tilde{N}} & \cdots & m_{2p+\tilde{N},\tilde{N}} \end{bmatrix}_{\tilde{N}\times\tilde{N}} \begin{bmatrix} l_1 \\ \vdots \\ l_q \\ \vdots \\ l_{\tilde{N}} \end{bmatrix} = \begin{bmatrix} m_{2p+1,1} \\ \vdots \\ m_{2p+1,q} \\ \vdots \\ m_{2p+1,\tilde{N}} \end{bmatrix}. \tag{3.8}$$

If a weighting update of a scalar coefficient is considered to be a linear subdivision, the update can be calculated using two ($\tilde{N} = 2$) neighbour wavelet coefficients, $d_{j+1,k-1}$

and $d_{j+1,k}$ (as shown in figure 3*a*). In this case, lifting factors are $l_1 = l_2 = \frac{1}{4}$, and the scalar coefficients can be updated to

$$a_{j+1,k} = A_{j,2k} + \tfrac{1}{4}(d_{j+1,k-1} + d_{j+1,k}).$$

This result is also equal to (2.14). When a weighting update of a scalar coefficient is considered to be a cubic spline interpolation, the update can be calculated using four neighbour wavelet coefficients. In this case, the lifting factors are $l = (-\frac{1}{32}, \frac{9}{32}, \frac{9}{32}, -\frac{1}{32})$, and the scalar coefficients can be updated to

$$a_{j+1,k} = A_{j,2k} + \tfrac{1}{32}(-d_{j+1,k-2} + 9d_{j+1,k-1} + 9d_{j+1,k} - d_{j+1,k+1}).$$

Three stages of wavelet transform are shown in figure 3*a*. The fast lifting wavelet transform algorithm is simplified to

$$\left.\begin{aligned} A_{j,2k}, A_{j,2k+1} &= \mathrm{Split}(A_j), \\ d_{j+1,k} &= A_{j,2k+1} - \rho(A_{j,2k}), \\ a_{j+1,k} &= A_{j,2k} + \mu(d_{j+1,k}). \end{aligned}\right\} \tag{3.9}$$

With this implementation of the forward wavelet transform, $z(x, y)$ has been driven to subsets $d_{j+1,k}$ and $a_{j+1,k}$, which record high- and low-frequency events at the scale $2^{-(j+1)}$ of $z(x, y)$. The whole decomposition of $z(x, y)$ is a simple repetitive scheme through rows and columns and all computations are done in-place. After j steps of decomposition in the scalar domain, an original surface signal $z(x, y)$ is replaced with the wavelet series $a_{j,k/2^{j-1}}$, $d_{1,k}$, ..., $d_{j,k/2^{j-1}}$. It can be expressed by

$$\begin{aligned} W_j[z(x,y)] &= (a_{1,k}, d_{1,k}) \\ &= (a_{2,k/2}, d_{1,k}, d_{2,k/2}) \\ &= (a_{j,k/2^{j-1}}, d_{1,k}, d_{2,k/2}, \ldots, d_{j,k/2^{j-1}}). \end{aligned} \tag{3.10}$$

Figure 3*b* shows this schedule, where j illustrates a decomposed level of wavelet transform in the scalar domain.

(*b*) *Separation and extraction of frequency components of a surface*

If a surface $z(x, y)$ is assumed to consist of a series of superimposed frequency components

$$z(x, y) = \eta(x, y) + \eta'(x, y) + \eta''(x, y), \tag{3.11}$$

these surface components can then be separated in the scalar domain by band-pass filters. The transmission bands are based on different cut-off wavelengths for different frequency components. As shown in the literature (Jiang *et al*. 1997*a*,*b*, 1999), wavelet coefficients $d_{1,k}$, ..., $d_{J,k/2^{J-1}}$ can be considered outputs of a high-frequency band $1/\lambda_s \sim 1/\lambda_c$, and refer to the roughness component $\eta(x, y)$. Here, $1/\lambda_s$ indicates the high frequency limited by the sampling interval, and $1/\lambda_c$ is the roughness frequency limitation. $d_{J+1,k/2^J}$, ..., $d_{j,k/2^{j-1}}$ represent the output (waviness $\eta'(x, y)$) of a sub-low-pass filter band $1/\lambda_c \sim 1/\lambda_{wc}$. $1/\lambda_{wc}$ is the waviness frequency limitation. The $a_{i,j/2^{i-1}}$ are scalar coefficients that represent the output (form error $\eta''(x, y)$) of a low-pass filter band $1/\lambda_{wc} \sim 1/l$, where l is the sample length when $l = l_x$ or l_y. Using an inverse wavelet transform, these surfaces can be recovered flexibly and immediately

in the different transmission bands in terms of functional analysis requirements. The inverse wavelet transform is performed simply by reversing the operation and toggling negative to positive for all operations:

$$\left.\begin{aligned}
\text{roughness:}\quad \eta(x,y) &= \mathrm{IW}(d_{1,k},\ldots,d_{J,k/2^{J-1}}) \\
&= \sum_{j=1}^{J}\{d_{j,k/2^{j-1}}(x,y)+\rho[A_{j-1,k/2^{j-2}}(x,y)]\}, \\
\text{waviness:}\quad \eta'(x,y) &= \mathrm{IW}(d_{J+1,k/2^{J}},\ldots,d_{j,k/2^{j-1}}) \\
&= \sum_{j=J+1}^{j}\{d_{j,k/2^{j-1}}(x,y)+\rho[A_{j-1,k/2^{j-2}}(x,y)]\}, \\
\text{form:}\quad \eta''(x,y) &= \mathrm{IW}(a_{j,k/2^{j-1}}) \\
&= A_{j-1,k/2^{j-2}}(x,y)-\mu[d_{j,k/2^{j-1}}(x,y)].
\end{aligned}\right\} \tag{3.12}$$

In order to obtain $\eta(x,y)$ and $\eta'(x,y)$, the scalar coefficients $a_{j,k/2^{j-1}}$ are set to zero and then backed out, and vice versa for $\eta''(x)$. In a similar way, a flexible reference surface can be obtained,

$$m(x,y)=z(x,y)-\eta(x,y)=z(x,y)-\mathrm{IW}(d_{1,k},\ldots,d_{J,k/2^{J-1}}). \tag{3.13}$$

If a functional evaluation of surfaces is needed to cover all of the topographical information from roughness, through multi-scalar events, to waviness, a functional surface can be built as follows:

$$\begin{aligned}
\eta(x,y)+\eta'(x,y) &= \mathrm{IW}(d_{1,k},\ldots,d_{j,k/2^{j-1}}) \\
&= \sum_{j=1}^{j}\{d_{j,k/2^{j-1}}(x,y)+\rho[A_{j-1,k/2^{j-2}}(x,y)]\}.
\end{aligned} \tag{3.14}$$

The identification of multi-scalar events in the bands of roughness and waviness is important in order to study the functional performance of the three-dimensional surface topography of many systems. These multi-scalar topographical events, $\xi(x,y)$, such as peaks/pits and rings/valleys, hide in the bands of roughness and waviness, and their wavelengths would cover a wide frequency range ($1/\lambda_{\mathrm{s}} \sim 1/\lambda_{\mathrm{wc}}$). Due to the fact that wavelet coefficient sets over the transmission bands have 'naturally' recorded the information concerning their amplitude and location, these events can be captured easily using an amplitude threshold T_j to pick out the roughness and waviness. Here, T_j is the value of an intersection of the probability curve of the cumulative amplitude distribution of each wavelet coefficient set referred to by ISO/DIS (13565-3, 1995).

This process is based on an assessment that the amplitude distribution of each wavelet coefficient set $d_{j,k/2^{j-1}}(x,y)$, belonging to roughness and waviness components, would obey the normal distribution. If the absolute value of the amplitude is equal to or larger than T_j, a thresholding estimator is applied,

$$d'_{j,k/2^{j-1}}=\begin{cases}0, & |d_{j,k/2^{j-1}}|<T_j,\\ d_{j,k/2^{j-1}}, & |d_{j,k/2^{j-1}}|\geqslant T_j.\end{cases} \tag{3.15}$$

Where the absolute value of the peak amplitude is smaller than T_j, the coefficient should be replaced by a zero. In the case of a detail coefficient being larger than or equal to T_j, the coefficient should be retained. As a consequence, detail coefficients that represent only the information of the topographical events are obtained. From the experiments carried out, the threshold approaches the standard deviation of each wavelet coefficient set. The multi-scalar topographic features can then be built by using the two-dimensional inverse discrete wavelet transform

$$\begin{aligned}\xi(x,y) &= \mathrm{IW}(d'_{1,k},\ldots,d'_{j,k/2^{j-1}}) \\ &= \sum_{j=1}^{j}\{d'_{j,k/2^{j-1}}(x,y)+\rho[A_{j-1,k/2^{j-2}}(x,y)]\}. \end{aligned} \tag{3.16}$$

4. Computer simulation

Before considering practical cases, it is useful to examine some profiles which comprise a number of harmonic components with different wavelengths. Although a synthetic harmonic signal is not a purely random waveform, it can be used to elucidate the transmission characteristics: *a brick wall, a linear phase and a traceably located property* of the lifting wavelet representation, and can then be compared with Gaussian filtering. The 'brick wall' is good for exact separation of different frequency components with a sharp attenuation at the cut-off wavelength; and a traceable location property can exactly mark transient signals throughout space. Two synthetic sinusoidal and triangular repetitive waveform profiles, each signal with five different wavelengths, $\lambda = (\frac{1}{3}, \frac{1}{2}, \frac{2}{3}, 1, 2)\lambda_c$, are used for digital simulation.

The synthetic waveform models are given by

$$\left.\begin{aligned} y_{\sin}(x) &= \sin\left(\frac{1}{\lambda_c/3}\cdot 2\pi x\Delta x\right)+\sin\left(\frac{1}{\lambda_c/2}\cdot 2\pi x\Delta x\right) \\ &\quad +\sin\left(\frac{1}{2\lambda_c/3}\cdot 2\pi x\Delta x\right)+\sin\left(\frac{1}{\lambda_c}\cdot 2\pi x\Delta x\right) \\ &\quad +\sin\left(\frac{1}{2\lambda_c}\cdot 2\pi x\Delta x\right), \\ y_{\mathrm{tri}}(x) &= \mathrm{tri}\left(\frac{1}{\lambda_c/3}\cdot 2\pi x\Delta x\right)+\mathrm{tri}\left(\frac{1}{\lambda_c/2}\cdot 2\pi x\Delta x\right) \\ &\quad +\mathrm{tri}\left(\frac{1}{2\lambda_c/3}\cdot 2\pi x\Delta x\right)+\mathrm{tri}\left(\frac{1}{\lambda_c}\cdot 2\pi x\Delta x\right) \\ &\quad +\mathrm{tri}\left(\frac{1}{2\lambda_c}\cdot 2\pi x\Delta x\right), \end{aligned}\right\} \tag{4.1}$$

with

$$\mathrm{tri}\left(\frac{2\pi x\Delta x}{\lambda}\right)=\begin{cases}\dfrac{2x\Delta x}{\lambda}, & -\frac{1}{2}\pi \leqslant \dfrac{2\pi x\Delta x}{\lambda} \leqslant \frac{1}{2}\pi, \\ \dfrac{1-2x\Delta x}{\lambda}, & \frac{1}{2}\pi \leqslant \dfrac{2\pi x\Delta x}{\lambda} \leqslant \frac{3}{2}\pi, \end{cases}$$

where x is the sampling number, Δx is the sampling interval and λ_c is a cut-off wavelength. The upper diagrams of figures 4*a* and 5*a* show the idealized input signals. Real filtered profiles can be found by using wavelet and Gaussian filtering with

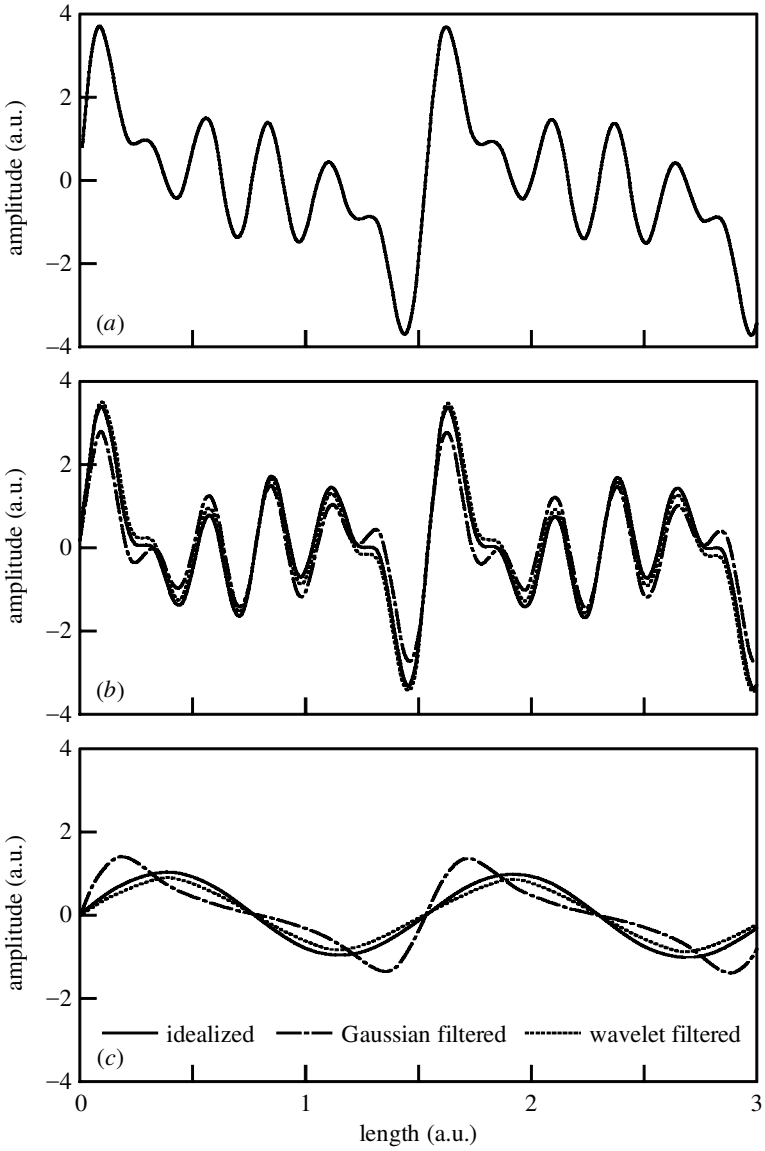

Figure 4. The transmission characteristic of a digital synthetic sinusoidal waveform by using Gaussian and wavelet filtering. (*a*) An idealized input waveform. (*b*) A comparison of the idealized and the real output waveforms. (*c*) A comparison of the idealized and the real mean lines.

the same cut-off wavelength λ_c (in figures 4*b* and 5*b*). The dotted line expresses an output of wavelet filtering, the dashed line is an output found by the Gaussian filter model, and the solid line is the ideal simulated output profile that is a combination of sinusoidal (triangular) repetitive waveforms with four different wavelengths, $\lambda = (\frac{1}{3}, \frac{1}{2}, \frac{2}{3}, 1)\lambda_c$. In figures 4*c* and 5*c*, the reference datum lines, obtained by ideal model and two kinds of filters, are given. The ideal mean lines are defined as a waveform with a single wavelength $2\lambda_c$.

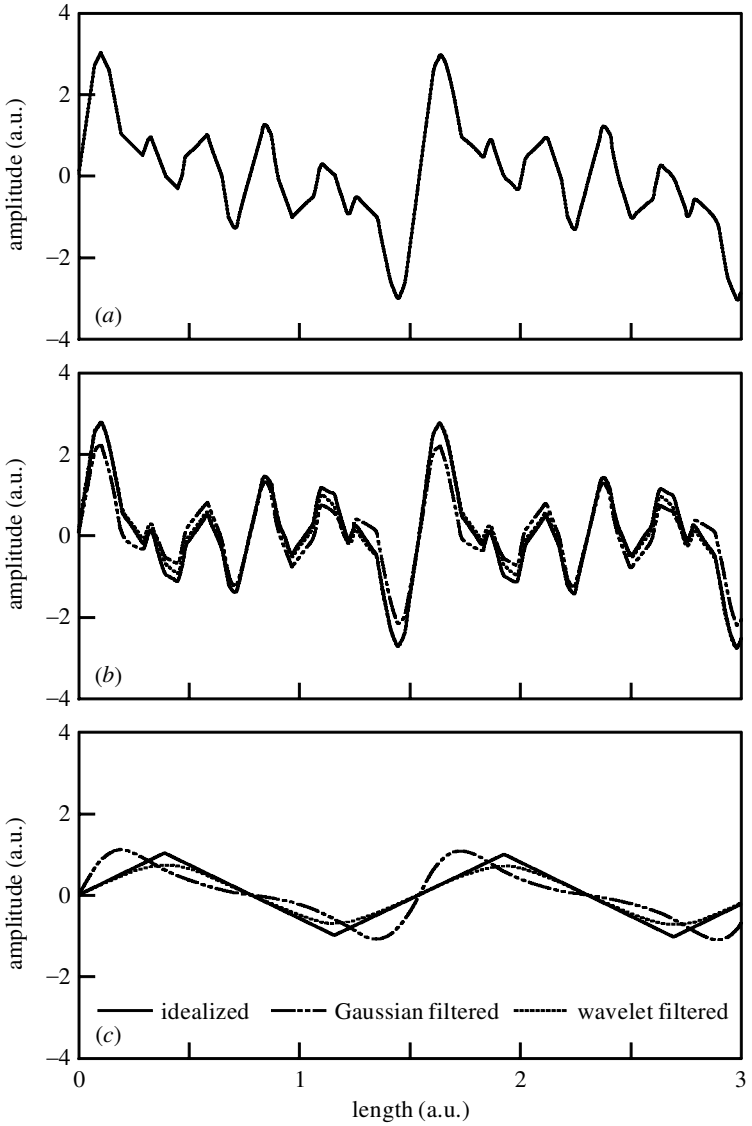

Figure 5. The transmission characteristic of a digital synthetic triangular waveform by using Gaussian and wavelet filtering. (*a*) An idealized input waveform. (*b*) A comparison of the idealized and the real output waveforms. (*c*) A comparison of the idealized and the real mean lines.

On comparison with the original input signals (in figures 4*a* and 5*a*) and idealized output signals (the solid lines of figures 4*b* and 5*b*), the outputs of the two filtering methods, the sinusoidal (triangular) waveform contents (the dashed and dotted lines in figures 4*b* and 5*b*), are not shifted relative to each other within the cut-off wavelength, and the components maintain their relative positions. The difference is that for wavelet filtering, the practically filtered profiles record the nature of sinusoidal and triangular waveforms, shape and amplitude, within a permitted cut-off

wavelength, with only a slight change in amplitude information, as expected. In other words, no distortion of the filtered profile is noted within this cut-off wavelength and, as a result, the sinusoidal and triangular waveforms have not suffered any attenuation for wavelengths up to the cut-off wavelength. The filtered mean profile is within a maximum value, 5% of the theoretical $2\lambda_c$ references (in figures 4*c* and 5*c*). It means an amplitude transmission characteristic is unified up to the cut-off wavelength and falls rapidly after the cut-off wavelength. Whereas for Gaussian filtering, harmonic amplitudes are modified in terms of the different attenuation ratios, all of which obey the Gaussian distribution, so that the output signals may include some artefacts information (in figures 4*b*,*c* and 5*b*,*c*). Contrary to this, the outputs obtained by employing wavelet filtering are more realistic.

5. Applications of the lifting wavelet representation

A large number of measurements of engineering surfaces (including turning, milling, reaming, grinding, ballising honing, lapping, polishing, electric discharging, rolling and chemistry processing) and topographies of bioengineering surfaces (such as super-lapping, diamond-like coating and UHMWPE), have been carried out. The accuracy of the surfaces of these components covers the levels from the micrometre to nanometre. The specimens originate from the standard specimens, real manufacturing process, running-in and worn specimens at a different stages. A group of typical examples of surfaces in engineering and bioengineering has been selected to show the behaviour of wavelet filtering. The measurement data of milled, ground and rolled surfaces and the reamed cylinder surfaces are generated by employing a Somicronic stylus instrument. The three-dimensional convex data from lapped ceramic and metallic femoral heads are produced using Wyko TOPO 3D and NT-2000 phase-shifting interferometers.

Figures 6 and 7 show decomposed examples of a rolled stainless steel sheet and a ceramic femoral head, respectively. Using only one operation of wavelet filtering, surface contents, roughness, waviness and form error can be detected and recognized. The outcomes of this are that the roughness surface $\eta(x, y)$, wavy surfaces $\eta'(x, y)$ and their corresponding form error surfaces $\eta''(x, y)$ can be immediately and perfectly reconstructed within a flexible transmission bank. For instance, in order to indicate this transmission flexibility, the cut-off wavelengths of roughness may be selected as $\lambda_c = 0.5$ mm for the rolled surface and $\lambda_c = 0.05$ mm for the ceramic head. The cut-off length of waviness is limited by practical applications. In the above examples, $\lambda_{wc} = 2.0$ mm is used for the rolled surface and $\lambda_{wc} = 0.10$ mm for the ceramic head.

Figure 8*a* shows six slope intensity images of general engineering and the ultra-precise bioengineering surfaces. The axonometric projections of their roughness surfaces, derived from two filtering methods, are shown in figure 8*b*,*c*. The cut-off wavelength λ_c of the two filtering methods is the same and based on the cut-off sample wavelength set down in the current British and International standards (BS 1134 (1996) and ISOs 4288 (1996) and 11562 (1994)). In this comparative study, the least-squares linear and quadratic polynomial fitting are used to remove irrelevant form and translation errors of flat and curved surfaces before Gaussian filtering implementation, according to Stout and Dong's suggestion (Stout *et al.* 1993; Dong *et al.* 1995), as well as to Sullivan & Luo (1989). It can be seen that when a measured raw datum of surface conforms the two assumptions of Gaussian filtering,

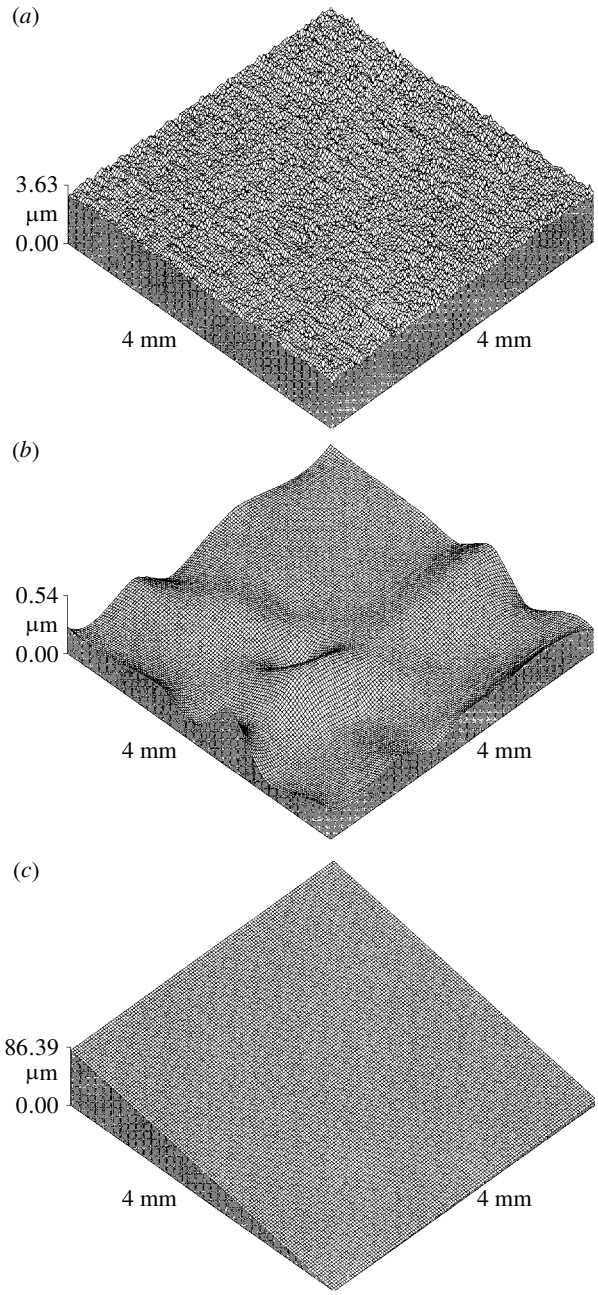

Figure 6. The decomposition of a rolled stainless steel sheet in different transmission bands by using wavelet filtering. (*a*) Roughness surface. (*b*) Wavy surface. (*c*) Form error surface.

the outcomes of the two filtering (in figure 8*b*,*c*) are similar to each other, without any relative phase shift in sampling area. The peak–valley information on the bearing surfaces conveyed is also recorded completely, with slightly modified amplitude in the Gaussian filtering case. This is similar to the standard repetitive waveforms

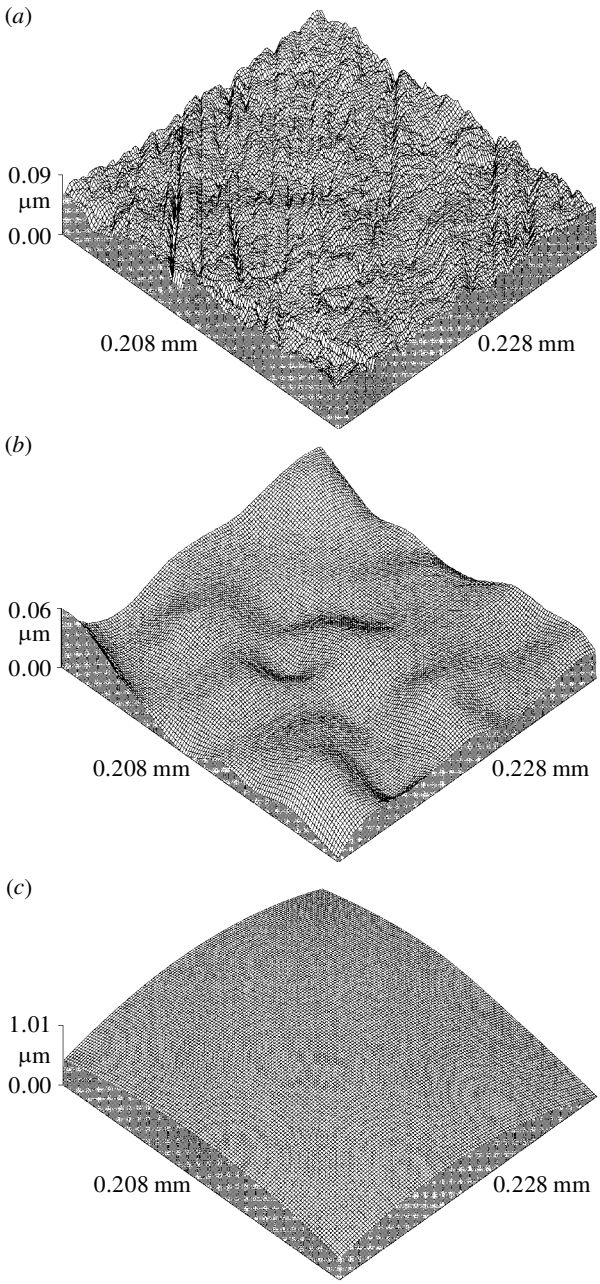

Figure 7. The decomposition of a lapped ceramic femoral head in different transmission bands by using wavelet filtering. (*a*) Roughness surface. (*b*) Wavy surface. (*c*) Form error surface.

displayed in figures 4 and 5. However, as far as surfaces with multi-scalar topographical features are concerned, and when the form error has not been removed by the least-squares polynomial fitting, the two filtering methods will give different results. Figure 8*a* shows four examples of these types of surfaces: a reamed surface with a

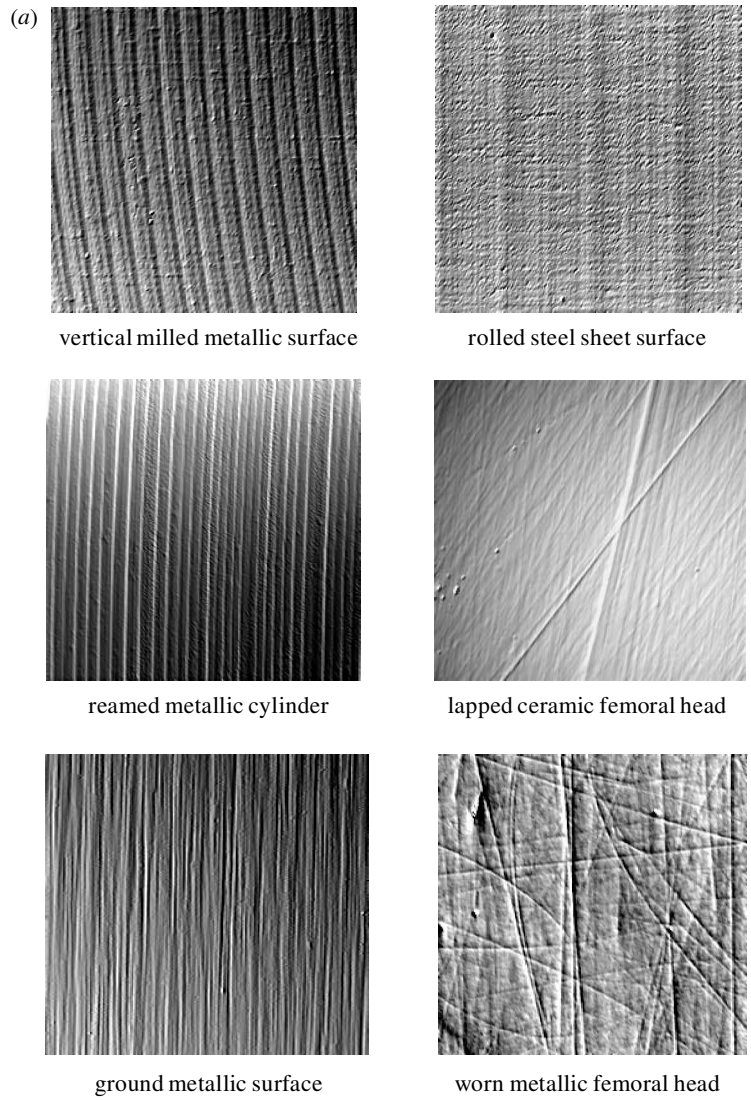

Figure 8. Analysis of the roughness of typical surfaces using a lifting wavelet filter and a Gaussian filter with least-squares polynomial fitting. (*a*) The typical bearing surfaces of engineering and bioengineering surfaces.

irrelevant form error, a rolled stainless steel sheet with large waviness energy near the cut-off length, and new ceramic and worn metallic femoral heads with multi-scalar frequency components. The results of wavelet filtering are better than those of Gaussian filtering (on the left of figure 8*b*,*c*). The roughness transmitted by the wavelet would appear to show only the roughness of the original surface from which the waviness, form and various errors have been removed, compared with those of Gaussian filtering. Examining the roughness of the centre profile taken across the roughness surfaces by Gaussian and wavelet models (shown in figure 8*c*), the results show that the components of roughness waveforms obtained by using Gaussian fil-

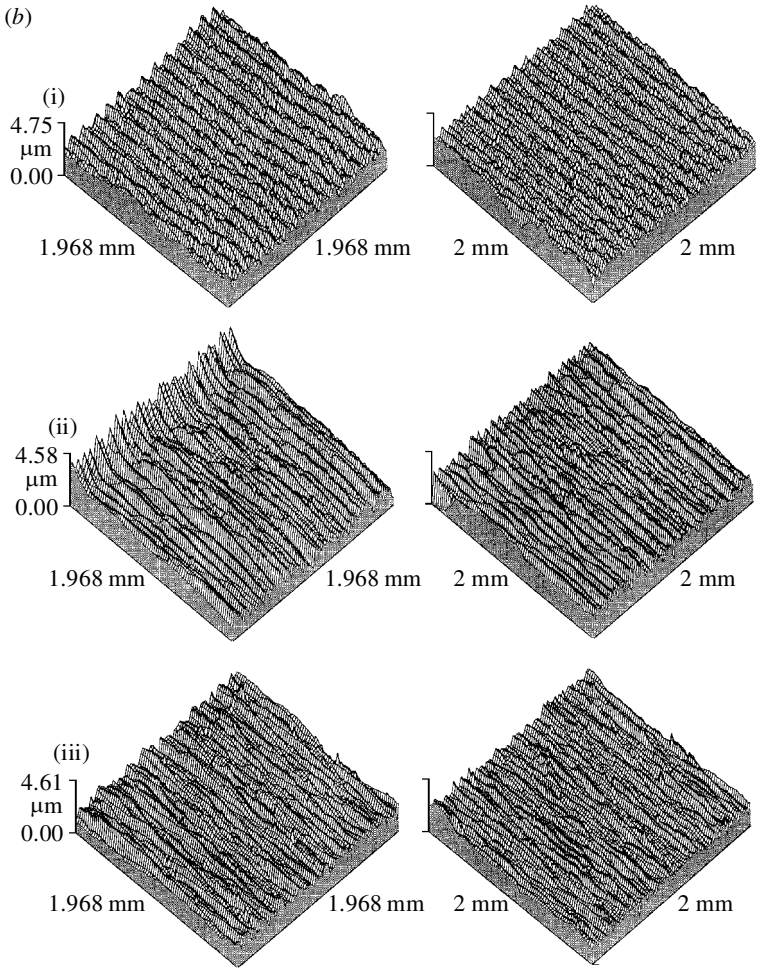

Figure 8. (*Cont.*) (*b*) A comparison of the residual surfaces (milled, reamed and ground) derived from (*a*) by employing Gaussian (on the left) and wavelet (on the right) filtering.

tering do not resemble those from wavelet filtering. The multi-scalar topographical features involved in roughness and waviness near the roughness cut-off length are not clearly eliminated, so that the obtained residual surfaces may give incorrect information. Therefore, it can be stated that for these types of surfaces, wavelet filtering is guaranteed to obtain a roughness surface with an excellent refinement accuracy. This accuracy is particularly suited to the need for highly accurate characterization of roughness parameters of three-dimensional surface topography.

In order to verify and provide practical evidence, the three-dimensional amplitude parameters of these specimens (in figure 8) are shown in table 2. Comparison of the results obtained using wavelet and Gaussian filtering is shown by two amplitude parameters, root-mean-square deviation Sq, and ten-point height of the surface Sz, and their relative variation. The parameter values are an average assessment (the three different parts of each engineering workpiece and the eight parts of each bio-engineering workpiece). From the results, it can be seen that when a measured raw

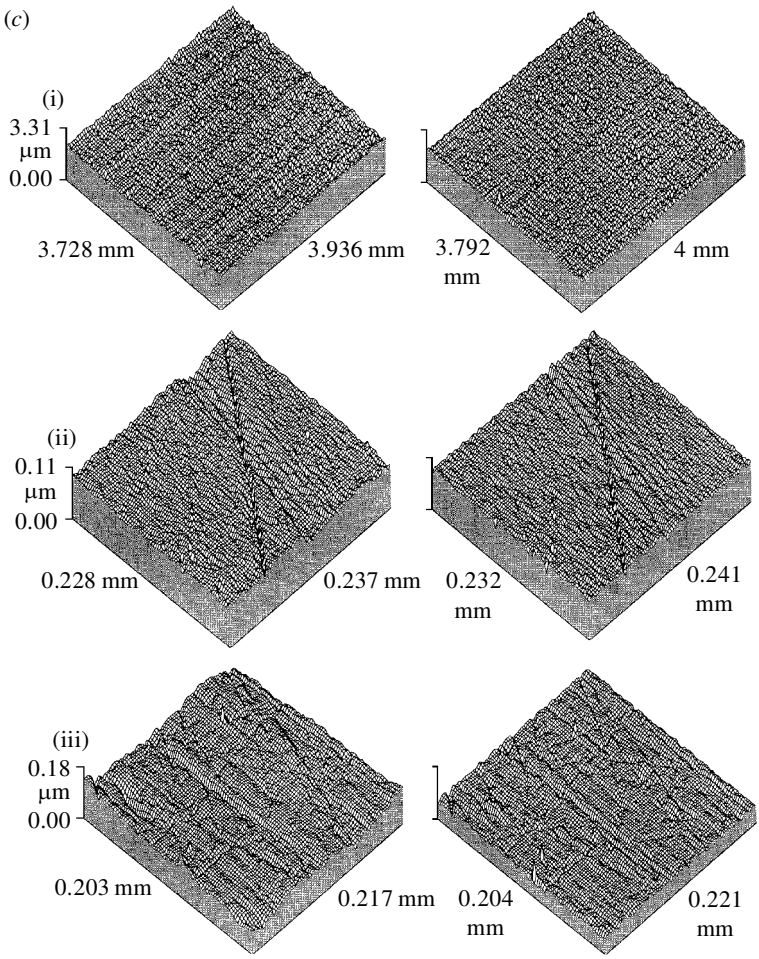

Figure 8. (*Cont.*) (*c*) A comparison of the residual surfaces (rolled, lapped and worn) derived from (*a*) by employing Gaussian (on the left) and wavelet (on the right) filtering.

datum of surface conforms to the two assumptions of Gaussian filtering, the parameter values achieved by wavelet filtering are similar to those from Gaussian filtering and the fluctuation of results of Gaussian filtering is a slightly larger than ones of wavelet filtering. However, as far as surfaces with multi-scalar topographical features are concerned, and when the form error has not been removed by the least-squares polynomial fitting, the amplitude parameter values obtained by wavelet analysis are clearly lower than those from Gaussian filtering, and the fluctuation of results is also obviously more stable. Considering the engineering surface, for instance, the ground metallic surface has $Sq = 0.457$ μm with a variation of 5% and $Sz = 3.618$ μm with a variation of 3% when analysed by wavelet analysis, but $Sq = 0.469$ μm with a variation of 21% and $Sz = 3.534$ μm with 11% variation are achieved from the Gaussian filtering. While for a bioengineering surface, the worn metallic head surface has $Sq = 2.639 \times 10^{-3}$ μm with a variation of 29% and $Sz = 2.980 \times 10^{-2}$ μm with 54% when assessed by wavelet analysis, but $Sq = 3.912 \times 10^{-3}$ μm with a variation of

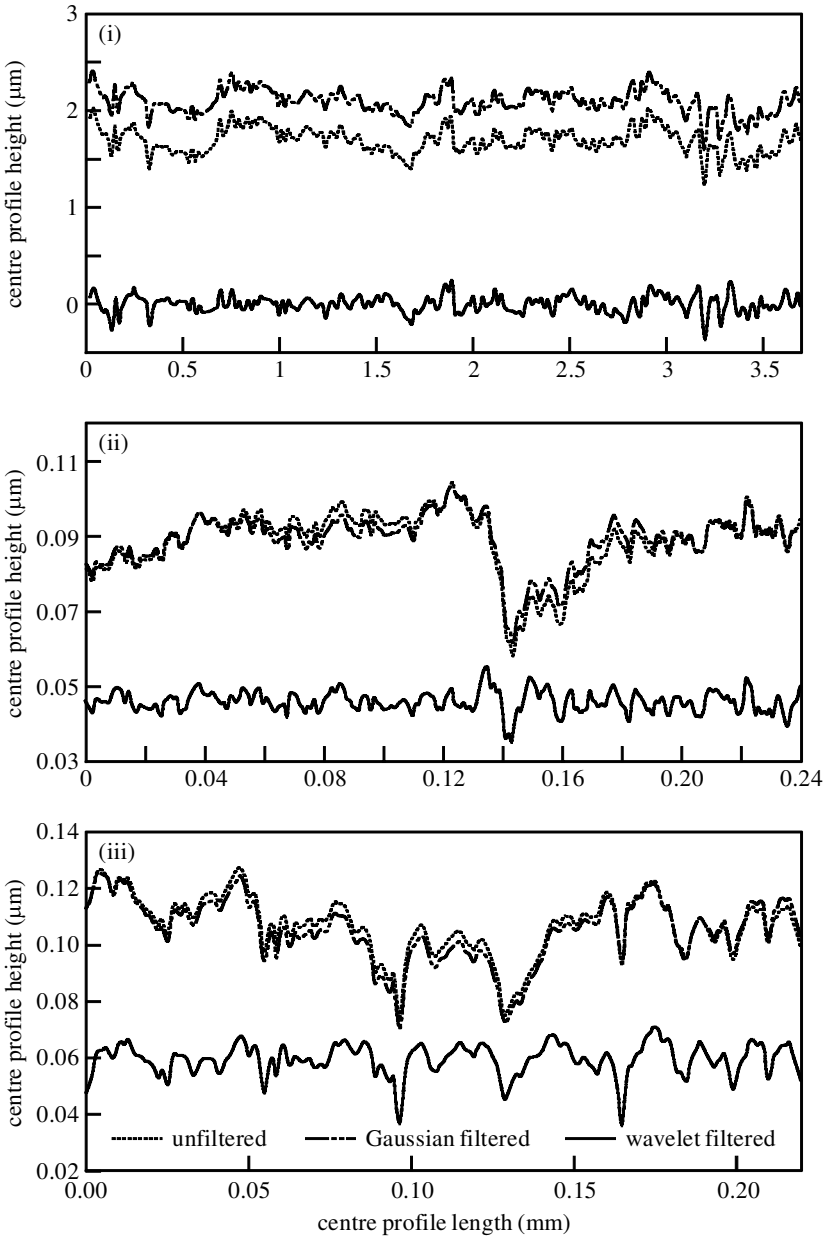

Figure 8. (*Cont.*) (*d*) The comparison of the centre profiles of roughness surfaces shown in (*c*).

49% and $Sz = 4.220 \times 10^{-2}$ μm with 96% when assessed from the Gaussian filtering. The main reason for the differences is that the residual surfaces fitted with Gaussian filtering include local random errors which are not components belonging to the roughness transmission band. In considering these results, it can be concluded that the areal parameter characterization generated by wavelet analysis is more stable and has a higher accuracy than that achieved using the Gaussian filtering technique.

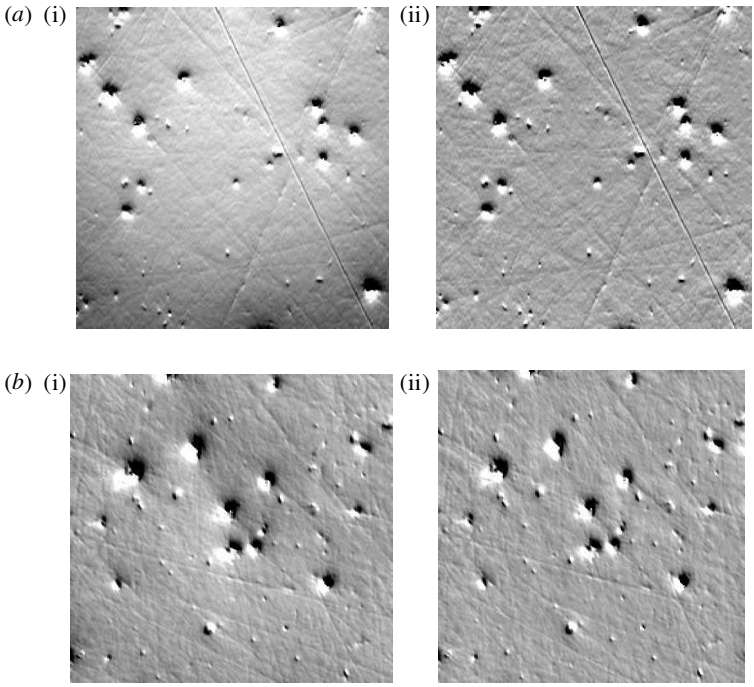

Figure 9. The polar and equatorial regions of the bearing surface of a new metallic femoral head. (i) The measured surface. (ii) The functional surface. (*a*) In the polar region. (*b*) In the equatorial region.

The following examples are used to highlight the surface texture derived from a new lapped femoral head and capture the functionally relevant topographical features derived from a worn head. The left-hand illustrations of figure 9*a*,*b* show lapped topographies in both the polar and equatorial regions of the new head with sampling area $300 \times 240\ \mu m^2$. The surfaces look 'fine and smooth' and have a 'classic' structure of random shallow scratches, isolated large pits and small peaks, and one-off deep scratches in the polar area. The right-hand images on figure 9*a*,*b* show how the wavelet model has removed form deviation revealing high quality functional surfaces. As illustrated, the multi-scalar topographic features are the dominant factors of the functional surface of this new head, and roughness and waviness may not influence the functional performance of the head in service due to their relatively low levels. As shown in figure 9*c*,*d*, traces taken from the polar region at random locations give strong evidence that using the new wavelet model, the significant features of functionally relevant topography can be naturally recorded and perfectly reconstructed. A further example is shown in figure 10. The left-hand illustrations of figure 10*a*,*b* show different parts of the bearing surface of a worn metallic femoral head. The surfaces have two different kinds of scratches: regular and shallow, possibly produced by manufacturing processing; and the random deeper scratches resulting from functional performance in service. The latter scratches have a wider frequency band and higher amplitude, some with arc structures. Using the segment property of the wavelet model in the scalar domain, functional surfaces, after form removal, are shown in middle of figure 10. The outcomes contain obvious waviness. The right-

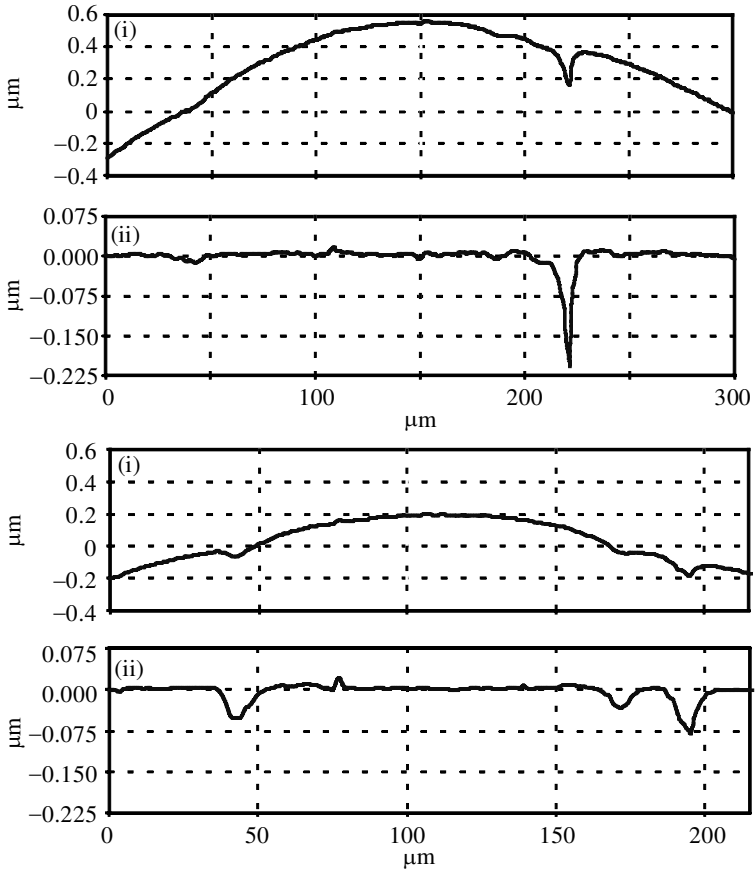

Figure 9. (*Cont.*) (*c*) A horizontal trace derived from the polar region. (*d*) A perpendicular trace derived from the polar region.

hand images of figure 10 highlight surface textures made up of multi-scalar events in which the roughness and waviness have been removed.

6. Conclusion

This paper has reviewed the existing numerical analysis methods and their problems in surface metrology. Based on this knowledge, this paper has proposed a novel, feasible and applicable tool, a lifting wavelet representation, for separation and extraction of different components of a surface. The theory of the lifting wavelet has been briefly introduced and a fast algorithm has been developed. The lifting wavelet has the following advantages when compared with the former techniques, Gaussian filtering and first-generation wavelet, from the point of view of theory and application.

(1) The theory of the lifting wavelet model is relatively new, simple and natural. The wavelet filtering process comprises three steps. The first is to decompose a surface original signal $z(x, y)$ to a sequence of subsets that transfers space-based information into scale-based information which represents both the frequencies of $z(x, y)$ and their location in scalar space. The second is to separate and

Table 2. *The average values and their variations obtained by a wavelet filter and a Gaussian filter*

3D amplitude parameters		a vertical milled metallic plane				a reamed metallic cylinder				a ground metallic plane			
		wavelet filtering		Gaussian filtering		wavelet filtering		Gaussian filtering		wavelet filtering		Gaussian filtering	
name	unit	average	variation	average	variation	average	variation	average	variation	average	variation	average	variation
Sq	(μm)	0.483	15%	0.50	21%	0.461	19%	0.476	27%	0.457	5%	0.469	21%
Sz	(μm)	3.852	6%	3.940	7%	3.314	10%	3.514	28%	3.613	3%	3.534	11%
3D amplitude parameters		a rolled steel sheet				a worn metallic femoral				a lapped ceremic femoral head			
		wavelet filtering		Gaussian filtering		wavelet filtering		Gaussian filtering		wavelet filtering		Gaussian filtering	
name	unit	average	variation	average	variation	average	variation	average	variation	average	variation	average	variation
Sq	(μm)	0.085	4%	0.131	20%	2.639×10^{-3}	29%	3.912×10^{-3}	49%	1.736×10^{-3}	12%	2.023×10^{-3}	42%
Sz	(μm)	1.818	22%	2.139	31%	2.980×10^{-2}	54%	4.220×10^{-2}	96%	2.300×10^{-2}	17%	2.700×10^{-2}	44%

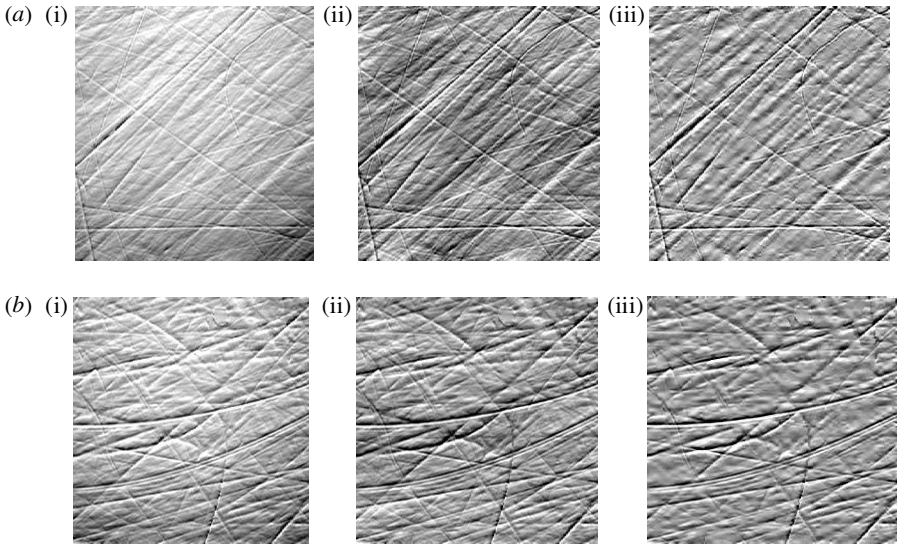

Figure 10. The polar and equatorial regions of the bearing surface of a worn metallic femoral head. (*a*) In the polar region. (*b*) In the equatorial region. (i) The measured surface. (ii) The functional surface. (iii) The multi-scalar topography.

capture the different frequency components involved in $z(x, y)$ within selected transmission bands. Finally, these different frequency surfaces can be reconstructed in the spatial domain.

(2) The wavelet transform algorithm is much easier and faster than conventional filtering methods, and the transform procedure only embraces three stages: 'plus', 'minus' and application of the weighting algorithm. All computations are carried out in-place through rows and columns, no extended memory is needed and the algorithm procedure is much faster than Gaussian filtering with least-squares polynomial fitting.

(3) The computer simulation shows the behaviour of wavelet filtering. Generally speaking, the filtered outputs derived resemble the idealized waveforms very closely without any shift relative to each other in a defined cut-off wavelength. As a result, the components have similar positions upon emerging from it. The peaks and pits are noticeable and can be preserved unambiguously. This is compared with Gaussian filtering, where, due to 50% of the intrinsic transmission characteristic of Gaussian filtering, the required frequency components can not be extracted clearly.

(4) The behaviour of the wavelet technique for surface analysis has initially been tested by experimental work. The given practical evidence shows that the filtered outcomes resemble the original waveforms very closely with no relative shift in the defined transmission band. As a result, the components have similar positions upon emerging from filtering and the peaks and valleys can be preserved unambiguously.

(5) Using the segment property in scalar domain, various surfaces can be flexibly, perfectly and immediately reconstructed according the intended requirements of functional analysis. The surface textures can be highlighted and multi-scalar topographical events can be identified and clearly recovered. The information obtained could be fed back to monitor the manufacturing processes, or to study actual contact stress, loaded area, asperity volume and lubrication regimes occurring during the initial stages of wear of surfaces in service.

The lifting wavelet model, and the corresponding algorithm allowing a better understanding of the three-dimensional surface, has been proposed. The different frequency components of surfaces can be considered and retrieved with the excellent refinement accuracy in the light of the algorithm. For industrial application purposes, the method has considerable merits. Practical examples have initially demonstrated the feasibility and applicability of the wavelet model.

We thank the European Community for support funds to carry out this work under its programme SMT CT98-2209. We also thank Dr P. J. Scott of Taylor Hobson very much for his advice concerning wavelet theory.

Nomenclature

$A_{j,k/2^{j-1}}(x,y)$	a two-dimensional discrete approximation of $z(x,y)$ at the scale 2^{-j}
$a_{j,k/2^{j-1}}$	scalar coefficients of $z(x,y)$ at the scale 2^{-j}
$d_{j,k/2^{j-1}}$	detail coefficients of $z(x,y)$ at the scale of 2^{-j}
$d'_{j,k/2^{j-1}}$	detail coefficients with a thresholding estimator
f_i	a set of filtering factors of the wavelet coefficient $d_{j,k/2^{j-1}}$
$g(k)$, $G(z)$	impulse and frequency responses of the two-channel synthesis filter
$h(k)$, $H(z)$	impulse and frequency responses of the two-channel analysis filter
$\mathrm{IW}[W(z(x,y))]$	the two-dimensional inverse wavelet transform
l_i	a set of lifting factors of the scalar coefficient $a_{j,k/2^{j-1}}$
j, k	a scalar parameter and a translation parameter (first-generation wavelet)
$m(x,y)$	a mean value (reference) surface of $z(x,y)$
M	an initial moment matrix for all data points at the first level
T_j	an amplitude threshold at the scale of 2^{-j}
$\mathrm{W}[y(x)]$, $\mathrm{W}[z(x,y)]$	a one- and two-dimensional wavelet transform
$y(x)$	a discrete signal
$y_{\sin}(x)$	a synthetic sinusoidal profile signal
$y_{\mathrm{tri}}(x)$	a synthetic triangular profile signal
$z(x,y)$	the discrete areal signal of the surface

$\eta(x,y)$, $\eta'(x,y)$, $\eta''(x,y)$	roughness, waviness and form error of $z(x,y)$
$\xi(x,y)$	multi-scale topography features of $z(x,y)$
$\tilde{\varphi}(x)$, $\varphi(x)$	analysis and synthesis scalar functions
$\psi(x)$	a prototype wavelet
$\psi_{j,k}(x)$	discrete basic wavelets
$\tilde{\psi}(x)$, $\psi(x)$	analysis and synthesis wavelet functions
λ_c, λ_{wc}	cut-off wavelengths of roughness and waviness
$\mu(d_{j,k/2^{j-1}})$	the weighting update of the scalar coefficient $a_{j,k/2^{j-1}}$
$\rho(a_{j-1,k/2^{j-2}})$	the weighting prediction of the wavelet coefficient $d_{j,k/2^{j-1}}$

References

Allen, J. B. & Rabiner, L. R. 1977 A unified approach short-time Fourier analysis and synthesis. *Proc. IEEE* **65**, 1558–1564.

Bachnick, M., Hasenpusch, M., Richter, H. & Boenick, U. 1994 The effects of hardness and surface quality of metal tapers on the fracture load of ceramic ball heads in hip endoprostheses. *Biomedizinische Technique* **39**, 302–306.

Bauer, T. W., Taylor, S. K., Jiang, M. & Medendorp, S. V. 1994 An indirect comparison of 3rd-body wear in retrieved hydroxyapatite-coated, porous, and cemented femoral components. *Clinical Orthopaedics Related Res.* **298**, 11–18.

Bhushan, B. 1996 *Tribology and mechanics of magnetic storage devices*, 2nd edn. Springer.

BS 1134 1990 *Assessment of surface texture*. British Standards Organisation.

Chen, X., Raja, J. & Simanapalli, S. 1995 Multi-scale analysis of engineering surfaces. *Int. J. Mach. Tools Manufact.* **35**, 231–238.

Chui, C. K. 1992 *An Introduction on wavelets*. Philadelphia, PA: SIAM.

Daubechies, I. 1988 Orthonormal bases of compactly supported wavelets. *Commun. Pure Appl. Math.* **41**, 909–996.

Daubechies, I. 1990 The wavelet transform time–frequency localisation and signal analysis. *IEEE Trans. Info. Theory* **36**, 961–1005.

Daubechies, I. 1992 *Ten lectures on wavelets*, 1st edn. Philadelphia, PA: SIAM.

Dong, W. P., Mainsah, E. & Stout, K. J. 1995 Reference planes for the assessment surface roughness in three dimensions. *Int. J. Mach. Tools Manufact.* **35**, 263–271.

Dyn, N., Gregory, J. A. & Levin, D. 1987 A four-point interpolatory subdivision scheme for curve design. *Computer Aided Geometric Design* **1**, 257–268.

Fisher, J., Dowson, D., Hamdzah, H. & Lee, H. L. 1994 The effect of sliding velocity on the friction and wear of UHMWPE for use in total artificial joints. *Wear* **175**, 219–225.

Flowers, B. H. 1995 *An introduction to numerical methods in C++*, 2nd edn. Oxford: Clarendon.

Gabor, D. 1946 Theory of communication. *J. IEE* **93**, 429–457.

Hall, R. M., Unsworth, A., Siney, P. & Wroblewski, B. M. 1996 The surface-topography of retrieved femoral heads. *J. Mater. Sci. Mater. Med.* **7**, 739–744.

ISO 11562 1994 *Surface texture—metrological characterisation of phase correct filters*. Geneva: International Standards Organization.

ISO 13565 1995 *Surface texture—characterisation of surface having stratified functional properties*. Geneva: International Standards Organization.

ISO 4288 1996 *Surface texture—rules and procedures for the assessment of surface texture*. Geneva: International Standards Organization.

Jiang, X. Q. & Li, Z. 1994 The development wavelet spectral analysis system for surface characterisation. NNSF no. 59375255, China.

Jiang, X. Q., Blunt, L. & Stout, K. J. 1997*a* Recent development in the characterisation technique for bioengineering surfaces. In *Proc. Metrology and Properties of Engineering Surface, Sweden, 2–4 April 1997*.

Jiang, X. Q., Blunt, L. & Stout, K. J. 1997*b* Evaluation of functional features of the orthopaedic joint prostheses surfaces using wavelet analysis. In *Proc. ASPE 1997 Spring Topical Meeting, Advances in Surface Metrology, Annapolis, Maryland*.

Jiang, X. Q., Blunt, L. & Stout, K. J. 1998 Wavelet framework representation for surface analysis (key note paper). In *Proc. 4th Int. Symp. of Measurement Technology and Intelligent Instruments, Miskolc, Hungary*.

Jiang, X. Q., Blunt, L. & Stout, K. J. 1999 Three-dimensional surface characterisation for orthopaedic joint prostheses. *Proc. Inst. Mech. Engng* **213**, 49–68.

Klimczak, T. & Hanzel-Powierza, Z. 1995 Application of the filter with dynamically controlled transmission band in surface texture analysis. *Ann. CIRP* **44**, 505–508.

Lee, S.-H., Zahouani, H., Caterini, R. & Mathia, T. G. 1998 Multi-scale analysis of engineering surfaces. *Int. J. Mach. Tools Manufact.* **38**, 581–589.

Liu, X., Raja, J. & Sannareddy, H. 1995 Assessment of plateau honed surface texture using wavelet transform. *Proc. ASPE* **14**, 672–675.

McGovern, T. E., Black, J., Graham, R. M. & Laberge, M. 1996 In-vivo wear of T16AL4V femoral heads—a retrieval study. *J. Biomedical Mat. Res.* **32**, 447–457.

Mallat, S. Q. 1989 A theory for multiresolution signal decomposition: the wavelet representation. *IEEE Trans. Pattern Analysis Machine Intelligence* **11**, 674–693.

Meyer, Y. 1993 *Wavelets: algorithms and applications*, 1st edn. Philadelphia, PA: SIAM.

Nayak, P. R. 1971 Random process model of rough surface. *Trans. ASME, J. Lubric. Technol.* **39**, 398–407.

Oliensis, J. 1993 Local reproducible smoothing without shrinkage. *IEEE Trans. Pattern Analysis Machine Intelligence* **15**, 307–312.

Rioul, O. & Vetterli, M. 1991 Wavelets and signal processing. *IEEE Signal Processing Mag.*, October, pp. 14–38.

Sato, H. & O-hori, M. 1981 Characteristics of two dimensional surface roughness taking self-excited chatter marks as objective. *Ann. CIRP* **30**, 481–486.

Scott, P. J. 1998 Trends in surface texture measurement. Technology toward the millennium, '98. MIRA Report, pp. 154–156.

Sherrington, I. & Smith, E. H. 1988 Fourier models of the surface topography of engineering components. *Surf Topography* **1**, 11–25.

Stoer, J. & Bulirsch, R. 1980 *Introduction to numerical analysis*, 1st edn. Springer.

Stollntz, E. J., Derose, T. D. & Salesin, D. H. 1996 *Wavelets for computer graphics*. San Francisco, CA: Morgan Kaufmann.

Stout, K. J., Sullivan, P. J., Dong, W. P., Mainsah, E., Luo, N., Mathia, T. & Zahyouani, H. 1993 *The development of methods for the characterisation of roughness in three dimensions*, 1st edn. Commission of the European Communities (ISBN 0 70441 313 2).

Strang, G. & Nguyen, T. 1996 *Wavelets and filter banks*, 1st edn. Wellesley, MA: Wellesley-Cambridge Press.

Sullivan, P. J. & Luo, N. 1989 The use of digital techniques for error correction in surface roughness measurement. *Surf. Topography* **2**, 143–157.

Sweldens, W. 1994 Construction and application of wavelets in numerical analysis. PhD thesis, Katholieke University, Leuven, Belgium.

Sweldens, W. 1995 *The lifting scheme: a custom-design construction of biorthogonal wavelets*. Murray Hill, NJ: Bell Laboratories.

Sweldens, W. 1996 *The lifting scheme: a construction of second-generation wavelets*. Murray Hill, NJ: Bell Laboratories.

Thomas, T. R. 1982 *Rough surface*, 1st edn. London: Longman.

Unswoth, A. 1995 Recent developments in the tribology of artificial joints. *Tribology Int.* **28**, 485–495.

Wallach, J. 1969 Surface topography description and measurement. In *Proc. ASME Symp. on Surface Mechanics, New York*.

Weszka, J. S., Dyer, C. R. & Rosenfeld, A. 1976 A comparative study of texture measures for terrain classification. *IEEE Trans. Systems Man. Cybernetics* **6**, 269–285.

Whitehouse, D. J. 1994 *Surface metrology*, 1st edn. Bristol and Philadephia: Institute of Physics Publishing.

Whitehouse, D. J. & Zhang, K. G. 1992 The use of dual space–frequency functions in machine tool monitoring. *Meas. Sci. Technol.* **3**, 796–808.

Wigner, E. 1932 On the quantum correction for thermodynamic equilibrium. *Phys. Rev.* **40**, 749–759.

Zhang, K. & Whitehouse, D. J. 1992 The application of the Wigner distribution function to machine tool monitoring. *Proc. Inst. Mech. Engng* **206**, 249–264.